Journal of
www. biophotonics-journal.org
BIOPHOTONICS

WILEY-VCH

J. Biophotonics **9**, No. 3, 224–234 (2016) / **DOI** 10.1002/jbio.201400145

Journal of BIOPHOTONICS

FULL ARTICLE

An infrared sensor analysing label-free the secondary structure of the Abeta peptide in presence of complex fluids

Andreas Nabers[**,1], *Julian Ollesch*[**,1], *Jonas Schartner*[1], *Carsten Kötting*[1], *Just Genius*[2], *Ute Haußmann*[2], *Hans Klafki*[2], *Jens Wiltfang*[2,3], *and Klaus Gerwert*[*,1]

[1] Protein Research Unit Ruhr within Europe (PURE), Ruhr-University Bochum, Department of Biophysics ND04-596, Universitätsstraße 150, 44780 Bochum, Germany
[2] Protein Research Unit Ruhr within Europe (PURE), LVR-Hospital Essen, Department of Psychiatry and Psychotherapy, Medical Faculty University of Duisburg-Essen, 45147 Essen, Germany
[3] University Medical Center, Department of Psychiatry and Psychotherapy, Georg-August-University, 37073, Göttingen, Germany

Received 2 December 2014, revised 19 February 2015, accepted 1 March 2015
Published online 24 March 2015

Key words: Amyloid-beta, neurodegeneration, label-free, ATR-FTIR spectroscopy, surface functionalization, complex mixture, body fluid, biosensor

The secondary structure change of the Abeta peptide to beta-sheet was proposed as an early event in Alzheimer's disease. The transition may be used for diagnostics of this disease in an early state. We present an Attenuated Total Reflection (ATR) sensor modified with a specific antibody to extract minute amounts of Abeta peptide out of a complex fluid. Thereby, the Abeta peptide secondary structure was determined in its physiological aqueous environment by FTIR-difference-spectroscopy. The presented results open the door for label-free Alzheimer diagnostics in cerebrospinal fluid or blood. It can be extended to further neurodegenerative diseases.

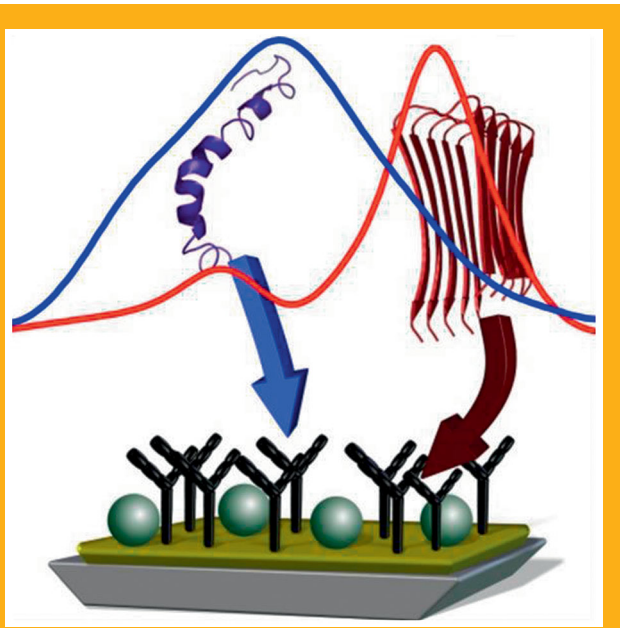

An immunologic ATR-FTIR sensor for Abeta peptide secondary structure analysis in complex fluids is presented.

* Corresponding author: e-mail: gerwert@bph.rub.de, Phone: +49 (0)234 32 29832, Fax: +49 (0)234 32 14849
** These authors contributed equally to this work.

1. Introduction

Protein misfolding and aggregation can be associated with a range of degenerative diseases including e.g. Alzheimer's (AD) or Parkinson disease (PD) [1]. Especially in neurodegenerative diseases, a secondary structure change of specific proteins into beta-sheet enriched conformations occurs [2]. However, most of such diseases are incurable, due to the diagnosis of late stages at which clinical symptoms become evident. At this stage, most of the alterations are irreversible. Therefore, diagnosis of early states is needed, if a therapeutic intervention will ever be successful.

AD is the most common dementia. It often becomes symptomatic around the age of 65 [3]. The typical clinical symptoms include progressive memory disturbances, disorientation, language difficulties and the impairment of judgment and decision making [4]. A multitude of factors triggering AD have been discussed [5]. According to the amyloid cascade hypothesis, an early and critical event in the onset of AD is the accumulation of Amyloid-beta (Abeta) peptides in the central nervous system [6–8]. Abeta peptides are proteolytically generated from the Amyloid Precursor Protein (APP) by beta and gamma secretases [9]. In human cerebrospinal fluid (CSF), five different carboxyterminal variants of Abeta comprising 37–40 or 42 amino acids, respectively, are routinely observed [10] with a total physiological concentration of approximately 15 ng/ml [11, 12]. In patients with AD, a selective decrease in Abeta42 in CSF is well documented [13] and inversely correlated with increased signals observed by PET amyloid *in vivo* imaging [14, 15]. This supports the idea, that Abeta can be used as diagnostic marker for an early state of the disease. The misfolding and aggregation of native soluble forms into oligomeric and fibrillar, beta-strand-rich structures have been proposed to be critically involved in the onset and progression of AD, where the beta-sheet-enriched disease states form characteristic plaques of amyloid fibrils [6, 16].

Especially the Abeta42 species shows a high propensity to aggregate [16]. The accumulation of toxic, oligomeric Abeta peptides is discussed to lead to neuronal cell death (e.g. pore forming, binding of bivalent ions, activation of apoptosis machinery) [17–19]. Oligomerization and fibrillation are accompanied with a structural transition to conformations enriched in beta-sheet secondary structures [20–22].

To determine such secondary structure changes, Fourier-transform infrared (FTIR) spectroscopy is a powerful tool. In particular, time-resolved FTIR-difference-spectroscopy demonstrated the excellent sensitivity of this technique. It is capable to resolve alterations of single residues within large protein-complexes by difference spectroscopy between different protein states. It revealed conformational changes and molecular reaction mechanisms of single residues within proteins with nanosecond time resolution at atomic detail [23, 24]. Out of the different possible molecular vibrations within a protein, the maximum frequency of the amide I band (1700–1600 cm^{-1}) caused by the C=O vibration of peptide bonds is indicative for the secondary structure of the protein backbone. This dependency has been extensively researched in simulation and experiment [25–30]. Alpha-helix and random coil to beta-sheet transitions are reliably detected by a frequency downshift of the amide I band from 1650 cm^{-1} to about 1622 cm^{-1} [31]. This was used for example to monitor the alpha-helix to beta-sheet transition of β_2-microglobulin fibril formation [32], and of lipid bound cellular prion protein [33]. Infrared microscopy demonstrated misfolded, beta-sheet enriched proteins in amyloid plaques of prion infected nervous tissue [34–36], a method patented for diagnosis of transmissible spongiform encephalopathies in tissues [37–39].

In order to monitor protein binding to lipid bilayers in aqueous environment, the attenuated total reflection (ATR) technique was frequently reported [33, 40–47]. In the ATR technique, an evanescent IR wave invades only few micrometers into the sample layers on the surface of the internal reflection element (IRE). On the surface of the IRE solid supported lipid bilayers (SSLB) are deposited. Thereby, strong absorbing liquid samples can be analysed in the IR, because only those molecules which are close to the surface are detected.

The surface can be nanostructured [48, 49] or chemically modified to enrich the analyte in the range of the evanescent wave [50, 51]. For the secondary structure analysis of a specific protein within a complex body fluid, the protein of interest has to be selectively and specifically bound to the surface. Here, this was achieved with an antibody-functionalized internal reflection element. The IRE was mounted within a customized flow-through-ATR-setup (see suppl. Figure 1 for schematics). The flow-through cuvette is covered with a quartz-window, which allows parallel control-measurements by fluorescence spectroscopy.

The sensor performance is demonstrated for the detection of synthetic Abeta peptides in single analyte solutions, cross-reactivity assays with albumin and alpha-synuclein, and the integral secondary structure analysis of the Abeta peptide species extracted out of a complex body-fluid-like solution.

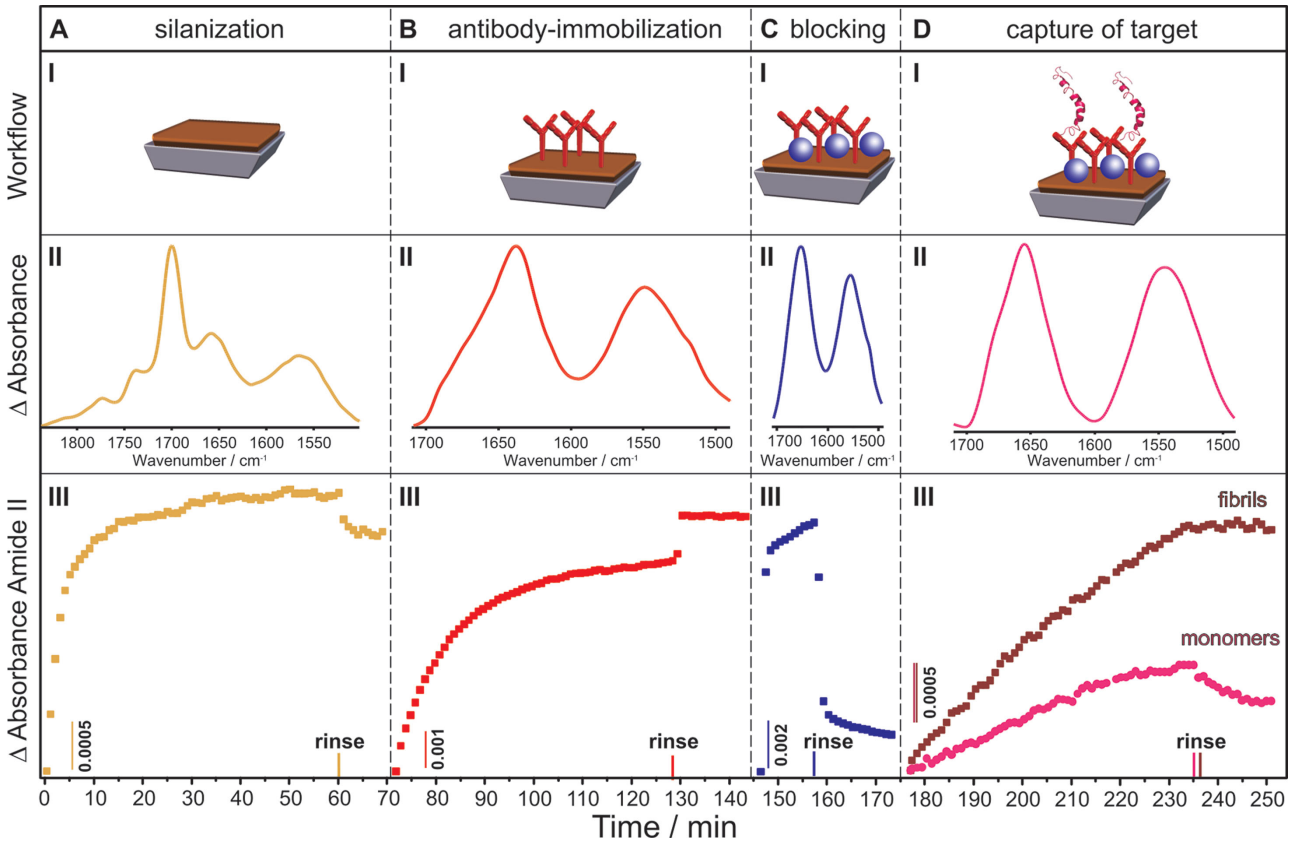

Figure 1 For all procedural steps (I) FTIR-spectra of the analytes were recorded after rinsing (II) and kinetic analyses of the amide II band were performed (III). The sensor surface was incubated with silane for 60 min. Unbound silanes were rinsed out (**A**). Similarly, the antibody modification was performed (**B**). Free reactive NHS groups were blocked with casein solution (**C**). Monomerized synthetic Abeta generated a typical amide I band of alpha-helical conformations (**D**II). Comparably, the binding kinetics of fibrillized Abeta peptides exhibited a stronger amide II intensity due to the capture of multimeric aggregates (**D**III).

2. Experimental

2.1 Workflow

Germanium IREs were polished, surface activated, silanized, loaded with Abeta capture antibody, and blocked. In a steady and defined flow, liquids were passed over the receptive surface. Infrared spectra were serially recorded. Using single channel spectra of defined states as reference, difference absorbance spectra of the preparative steps were calculated. For the validation of the different preparative steps, difference absorbance spectra (Figure 1) and fluorescence signals (Figure 3) were recorded.

2.2 Instrumentation

A Vertex 70v FTIR-spectrometer (Bruker Optics GmbH, Ettlingen, Germany), equipped with a liquid N_2 cooled mercury cadmium telluride (MCT) detector and water cooled, high efficiency MIR source was used. The ATR unit "GS11000 – 25 Reflection Variable Incidence Angle ATR" (Specac Ltd., Slough, England) was mounted in the internal sample compartment, adjusted to a 45° incidence angle. A trapezoid germanium ATR-crystal (52 mm × 20 mm × 2 mm, Korth Kristalle GmbH, Altenholz (Kiel), Germany) was used as IRE. The internal sample compartment was thoroughly purged with clean and dry air (Purge air generator Model 75-62-12VDC, Parker Hannifin Corp., Haverhill, MA, USA) at a rate of 800 l/h. The IRE housing was custom engineered as a stainless-steel flow cuvette optimized for a flow-covered area of 1500 mm^2. One side was equipped with a quartz-window for optical control. Constant liquid flow of 1 ml/min was provided with a peristaltic pump (Ismatec Reglo Digital, IDEX Health&Science, Wertheim-Mondfeld, Germany). The total system volume was determined as 1 ml.

2.3 Chemicals

All chemicals used were of analytical grade. Phosphate buffered saline (PBS) buffer solution consisted of 137 mM sodium chloride (J. T. Baker), 2.7 mM potassium chloride (VWR), 12 mM total-phosphate (Na_2HPO_4/NaH_2PO_4, J. T. Baker), pH 7.4. The reaction-phosphate buffer was an aqueous solution of 50 mM Na_2HPO_4/NaH_2PO_4, pH 8.0. The silane N-4,4,4-Triethoxysilanebutyl succinamic acid 2,5-dioxopyrrolidin-1-yl ester was synthesized and characterized as described [52]. Hydrogen peroxide was obtained from J. T. Baker, and oxalic acid from Sigma Aldrich. The method was established with monoclonal antibody 1E8 (Merck Millipore, Darmstadt, Germany). For fluorescence detection, fluorescein isothiocyanate (FITC)-labeled 8G7 antibody (Nanotools, Antikörpertechnik GmbH, Teningen, Germany) was used.

2.4 FTIR spectrometer parameters

Double-sided interferograms were recorded in forward-backward interferometer movement at a 60 kHz data rate with a spectral resolution of 2 cm^{-1}, Blackman-Harris-3-Term-apodisation, Mertz-phase correction and 4 times zero filling. Reference spectra were recorded as an average of 1000, sample spectra of 200 interferograms.

2.5 ATR crystal preparation

For each binding experiment, the Ge-IRE was bilaterally polished with 0.1 µm grained diamond grinding suspension for 5 min (Struers A/S, Ballerup, Denmark). The crystal was incubated three times in a hydrogen peroxide/oxalic acid mixture (9 : 1) for 5 min, rinsed with water between every incubation step and dried with nitrogen gas.

2.6 Sensor surface modification

The sensor surface was incubated with 300 µM silane solution in 2-propanol for 60 min, unspecifically linked silane was removed by rinsing with 2-propanol for 15 min. After media change to the reaction buffer, 100 ng/ml antibody solution was flushed over the activated silane surface until saturation, monitored by the immobilization kinetics of the amide II band of the antibody. Unspecifically bound antibodies were rinsed out with PBS-buffer until an equilibrium of their amide II absorbance was achieved. Free reaction sites of the sensor surface were saturated with 1% w/v casein (Sigma-Aldrich) in PBS buffer followed by rinsing with PBS buffer.

2.7 Fluorescence analysis

For fluorescence labelling, a second FITC-labeled 8G7 antibody at a final concentration of 5 ng/ml was added into the cuvette within a circulated flow. The binding of the detection antibody to immobilized Abeta peptides was monitored by the amide II absorbance between 1600 and 1500 cm^{-1}. After saturation was reached, unbound antibody was removed by buffer rinsing. Fluorescence intensity at 518 nm was recorded as the average intensity (integrated RGB intensity value of the green channel) of five 420 × 420 μm^2 regions, within a randomly selected area of 1073 × 1428 μm^2, excited at 484 nm (X-cite 120Q UV-laser, Lumen Dynamics Group Inc., Canada) and exposed 1 s at 1,000 fold magnification in a fluorescence microscope (Olympus BX41, camera XC10).

2.8 Spectral preprocessing

Spectral traces of atmospheric water vapour were removed by scaled subtraction of a reference spectrum. High frequency noise with a full width at half height (FWHH) of less than four wavenumbers was removed by a Fourier low pass filter [53].

Spectral contributions of liquid water molecules in the amide I band were removed by a scaled subtraction of a reference buffer absorbance spectrum to achieve an even baseline between 1750–1700 cm^{-1} for secondary structure analysis. Further, the contribution of amino acid side chains on the amide I band of Abeta-peptide was eliminated through a side chain correction [31].

For details about the signal to noise ratio (S/N) determination, please see the supplement.

For a quantitative analysis of binding kinetics, the amide II band was used. This band is not affected by the water absorbance and used as an additional control for water band subtraction.

Kinetic analyses were performed after baseline correction of all spectra. Therefore, the absorbance was set to zero at two interpolation points between 1850–1860 cm^{-1} and 2200–2210 cm^{-1}.

2.9 Analysed samples

Lyophilised synthetic Abeta42 (Bachem AG, Bubendorf, Switzerland) was dissolved in hexafluoroi-

sopropanol (HFIP) at a concentration of 2 mg/ml over night at room temperature, and aliquoted to 100 µg. HFIP was removed by evaporation for 60 min in a centrifugal evaporator (Concentrator plus, Eppendorf, Hamburg, Germany) at RT and 20 mbar.

The protein film was dissolved in phosphate buffer (50 mM Na_2HPO_4/NaH_2PO_4, pH = 8) and vortexed until a clear solution was obtained. For the analysis of monomeric Abeta, the solution was analyzed within 1 h after protein suspension in aqueous buffer. A fibril suspension was identically started with monomerised peptide. After dissolving the protein in buffer, the solution was incubated at 37 °C, shaking at 350 rpm (Thermomixer, Eppendorf) for at least 24 h. Fibrils were harvested by 30 min centrifugation at 13,000 g, discarding the supernatant, and gentle resuspension of the pellet in PBS buffer. Protein concentrations were verified spectrometrically [54].

Primary telencephalon neuronal cells from chicken embryo were prepared and cultivated in a commercial Neurobasal Medium (Gibco, Thermo Fisher), supplemented with 0.5 mM L-glutamine and B27/-AO supplement as described previously [55]. These cells express the Amyloid Precursor Protein (APP) and secrete a pattern of Abeta peptides comprising Abeta37, 38, 39, 40, 42 [56]. The cell-free supernatant was collected on DIV 4 centrifuged at 30,000 g for 30 min and stored at –80 °C until FTIR-analysis.

3. Results and discussion

For the detection and secondary structure analysis of Abeta peptides selected from liquid samples, a novel ATR-FTIR based immuno-sensor was developed. The main element of the new sensor is an ATR-flow-through cuvette, equipped with a germanium-(Ge) crystal (1,500 mm^2 effectively functionalized surface) as an internal reflection element (IRE). For the analysis of specific proteins from complex samples, the crystal surface of the IRE had to be modified. Liquids circulate with a flow rate of 1 ml/min within the custom-build ATR-flow-through system. This enabled the detailed evaluation of each single procedural step with difference absorbance spectra (Figure 1). A single channel reference spectrum I_0 was recorded from a rinsed surface. After sample application, unbound sample was rinsed out, and a single channel spectrum I was recorded. The sample absorbance A was calculated using $A = -\log (I/I_0)$.

The surface modification by triethoxysilanes with an *N*-hydroxysuccinimidyl ester (NHS) linker (Figure 1AI, II, III) was described in detail [52]. Briefly, the linker silane bound to the IRE (Figure 1AII), whereas after 60 minutes, unbound silane molecules were rinsed out (Figure 1AIII). Consecutively, the monoclonal 1E8 antibody is bound to the silane via free amine groups such as present in exposed lysine side chains (Figure 1BI, II, III). The antibody remained reactive for more than 17 days when stored at 4 °C (suppl. Figure 2). The 1E8 antibody captures the Abeta peptide by the N-terminal part out of liquid samples. The amide I and amide II bands of the antibody are shown in Figure 1BII. The time course of 1E8 binding indicated an absorbance increase after rinsing due to buffer differences. This is the so called swelling effect (Figure 1BIII).

The surface coverage with antibody 1E8 was monitored using the amide II band (Figure 2). In a concentration series, the optimal antibody amount required was determined. Thereby, surface saturation was achieved with 100 ng within the total sensor volume of 1 ml. 200 ng/ml lead to the same surface coverage in contrast to lower concentrations (Figure 2). Thus, the surface was coated in further experiments at an antibody concentration of 100 ng/ml. A moderate absorbance increase was detected after rinsing with running buffer for low antibody concentrations, but increases at higher concentrations were mainly caused by different buffers and ionic strength. However, the antibody layer is stable during rinsing.

The potentially remaining reactive surface of the IRE was saturated with casein as blocking protein (Figure 1CI, II, III) in order to avoid non-specific protein binding at the surface when complex fluids are floated over the IRE. The increase of the amide II absorbance during loading the system with casein solution and the decay of the signal is caused by buffer rinsing. The final amide II absorbance of 1.5×10^{-3} indicated both a predominant coverage of the surface

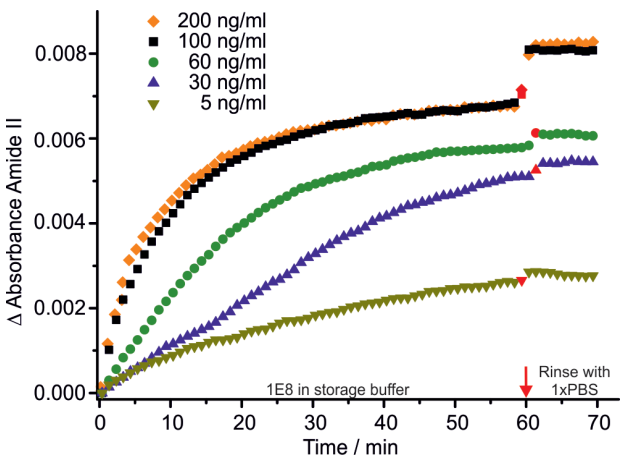

Figure 2 The amide II absorbance increase indicated surface immobilization of antibody 1E8 on the silanized ATR-IRE. After 60 min incubation, unbound antibody was rinsed out with PBS buffer, causing an abrupt absorbance increase due to altered buffer conditions. The constant signal during rinsing indicated the presence of a stable antibody layer on the IRE.

with antibodies (6.25×10^{-3}) and successful immobilization of casein on the IRE surface (Figure 1CIII). The blocking by casein is crucial for the specificity of Abeta binding (suppl. Figure 3). In steps A to C, the IRE surface was prepared to achieve the exclusive receptivity of the 1E8 antibody against Abeta or Abeta related proteins such as sAPPalpha, a non-amyloidogenic fragment of the APP cleaved by alpha-secretase after amino acid K687 (Abeta sequence K16). The 1E8 antibody is specific for the N-terminal part of the Abeta peptide [56, 57] independent of its secondary structure. The selective binding

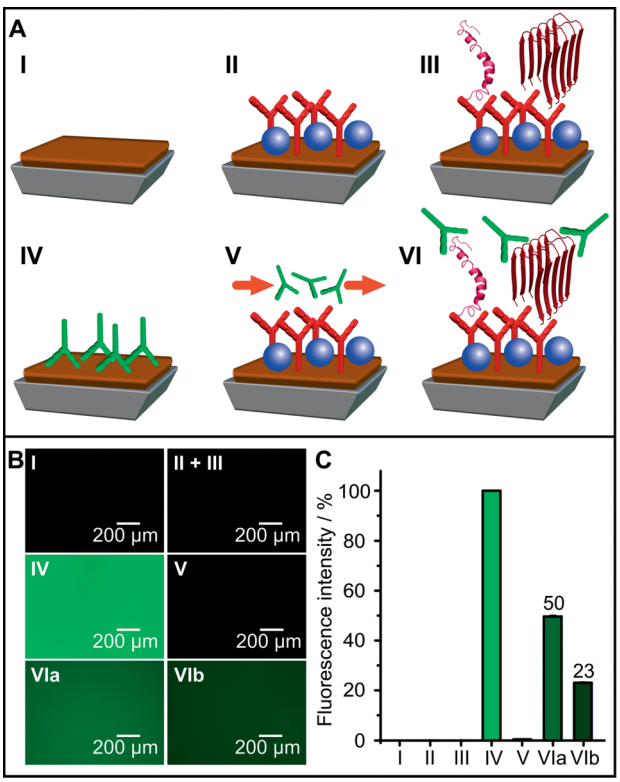

Figure 3 (**A**) Schematic setup of the FTIR-experiment (I–III) and fluorescence controls (IV–VI). The IRE surface of the home-made-flow-through ATR setup was modified (I) to covalently bind analyte-specific antibodies (red Y-shapes, II). Remaining binding sites are blocked with casein (blue spheres). The analyte is specifically captured by the antibodies from a complex solution (III). (**B**), the fluorescence signal of a secondary labeled antibody (8G7-FITC, green) are shown for steps I–VI (**C**). Fluorescence intensities are shown: neither the silane surface (I), nor the primary antibody 1E8 and casein (II), nor bound Abeta peptide (III) yielded any fluorescence background. As expected, 8G7-FITC itself, directly immobilized on the surface, showed a signal (IV), which was used as 100% reference. 8G7-FITC did not bind to the functionalized sensor surface (V). The fluorescence signal of 8G7-FITC indicated the binding of synthetic Abeta peptide (VIa) and the successful binding of Abeta extracted out of neuronal cell-culture medium (VIb).

of Abeta was achieved by circulating the Abeta containing sample over the antibody-functionalized IRE for 60 min (Figure 1DI, II, III). The system contained 1 ml buffer in the rinsed state. Adding a protein solution dilutes the sample accordingly. Because a sample can circulate within the system, small volumes of 20–100 µl are sufficient for an analysis. If insufficient binding is detected, more sample can be added until a satisfactory S/N is reached (Figure 1DIII). Assuming 15 ng/ml total Abeta concentration in a CSF sample, about 71 µl CSF had to be added to reach the detection limit of 1 ng/ml of the presented sensor. This is a small volume suitable for clinical application. In Figure 1DII, the amide I and amide II band of synthetic Abeta attached to the surface are shown. The unbound monomer and fibril protein fraction was rinsed off with an appropriate buffer solution (Figure 1DIII). Both monomeric and fibrillar peptides were successfully captured. This demonstrated that the antibody 1E8 is not selective for a specific secondary structure, as expected. The fibrils were bound tighter than the unfolded/alpha-helical Abeta peptides, as indicated by their amide II band decrease during rising. In beta-sheet fibrils, more epitope binding is possible, which explains the tighter binding.

For validation of specific Abeta binding, parallel fluorescence analyses were performed (Figure 3). The fluorescence signal of FITC-labeled 8G7 antibody indicated binding to the C-terminus of the Abeta42 peptide (Figure 3AVI). 1E8 captures Abeta peptides with the N-terminal epitope 1–2. Though, 8G7 is an ideal indicator of Abeta42 peptide, because it does not recognize the major cross reactand sAPPalpha. Therefore, 8G7 confirmed the successful binding of synthetic and neuronal Abeta selected out of a complex fluid (Figure 3B VIa and b). Compounds used to functionalize the sensor surface did not show any inherent fluorescence signals (Figure 3I, II, III). Furthermore, the controls indicated that 8G7 was bound directly to the reactive IRE (Figure 3IV), but not to the antibody-functionalized sensor surface without Abeta (Figure 3V). Thus, all remaining potential binding sites after covalent binding of the first antibody were inactivated by casein. The binding of the synthetic Abeta42 peptide, as indicated by fluorescence, demonstrated a higher fluorescence intensity than the Abeta selected out of the neuronal cell-culture media (Figure 3CVIa and b). Most likely, this was due to surface coverage by Abeta peptide variants not recognized by 8G7.

In the next step, the recorded Abeta peptide amide I bands were analyzed to determine the secondary structure. The corresponding amide I bands of monomeric and fibrillized synthetic Abeta peptide samples showed the expected characteristic signatures. The monomeric protein was dominated by alpha-helix under the given measurement conditions

(Figure 4A), amyloid fibrils (Figure 4B) [58–60] were dominated by beta-sheet. It is obvious, that the alpha-helix/ random coil conformation of the Abeta peptide in the healthy state can clearly be distinguished from beta-sheet conformation in the diseased state. However, a more detailed secondary structure analysis by deconvolution of the FTIR amide I band into the different secondary structure components was also performed. Because the deconvolution is not unique, the deconvolution was calibrated using the NMR secondary structure data of the monomeric Abeta42 peptide. This was introduced for prion proteins [31]. Curve fitting of the amide I band is an underdetermined problem. Initialization parameters for the fitting procedure were adjusted, that the result matched the NMR-data of the monomeric peptide [61]. The determined four structure elements exhibited a root mean squared deviation (RMSD) of ±4 %. The analysis procedure was validated with the absorbance spectrum and NMR data of the fibrillar state [62]. The comparison yielded an RMSD of ±5%. We take this as the estimated error of the curve fitting analysis (Table 1). Although each experiment requires the preparation of an entire sensor, the recorded spectra are extremely reproducible (suppl. Figure 4).

The monomeric Abeta peptide was characterized by an amide I band maximum intensity at 1655 cm^{-1}, indicating an alpha-helical secondary structure (Figure 4A). Under the preparation conditions used, the Abeta peptide showed an alpha-helical content of 46% in agreement with a NMR study. However, using different buffer conditions and resolvents, the Abeta peptide may exist in unfolded states as determined in different NMR-studies [63–65]. Here, under the selected buffer and Abeta concentrations, no refolding of Abeta peptides was observable. Amyloid fibrils displayed a downshift to 1628 cm^{-1} with a second band at 1664 cm^{-1} indicating clear-cut beta-sheet structures (Figure 4).

The signal expected in body-fluids will be smaller than for these two artificial compounds representing the most extreme cases.

Therefore, the performance of the set-up for secondary structure analysis of Abeta extracted from a complex, body-fluid-like biological sample was demonstrated. For that purpose, cell-free conditioned media from telencephalic chicken neuronal cell-culture was analysed. It contained an undetermined mixture of proteins and metabolites from the cultured cells, and an Abeta peptide pattern and concentration similar to those found in human CSF [66], which is the most important body fluid for neurochemical dementia diagnosis.

Abeta peptides were captured from the neuronal cell-culture medium as described in Figure 1. In addition, the binding of the Abeta peptide was supported by fluorescence control measurements (Figure 3VIb). The amide I band of cell-culture Abeta demonstrated an excellent S/N for a reliable secondary structure determination with physiological Abeta peptide concentrations, even when isolated from a complex medium. Its amide I band is similar to the synthetic Abeta monomer amide I band (Figure 4A, C). The spectral decomposition of the neuronal Abeta amide I band into a linear combination of the spectra recorded of the synthetic monomer and fibril yielded a mixture of a 92% monomeric and 4% fibrillar fraction in the cell-culture supernatant. The integrated not determined residual component represented 4% of the total signal. This unexplained residual could be caused by oligomeric Abeta or the Abeta related protein sAPPalpha (suppl. Figure 5). Here for the first time, the secondary structure of the Abeta peptide as present in an unprocessed complex physiological solution is measured with sufficient S/N ratio, which allows a secondary structure analysis in the presence of the aqueous body fluid. Thereby, the Abeta peptide secondary structure in the healthy and disease states can be determined directly in body fluids.

In a next step, different concentrations of synthetic Abeta42 peptides were measured to determine the minimum amount which can be usefully detected by this approach (Figure 5A). Small amounts of peptide were added stepwise to the buffer-filled flow system to achieve the given total concentration in the total system volume. Beside the amide I (1649 cm^{-1}) also the amide II band (1547 cm^{-1}) is shown. The amide II band is mainly caused by the peptide backbone N–H-bending vibration. It was used as an alternative to the amide I band, which is

Table 1 Secondary structure analysis of monomerized and fibrillar synthetic Abeta42 protein as compared with NMR structures (PDB 1Z0Q, 2BEG), and the Abeta peptide fraction released into culture medium by primary neuronal cells from chicken embryo. For the FTIR analysis of Abeta in culture medium, an error of 5 % is estimated from the RMSD of NMR and FTIR results on the fibrillar state.

structure element	monomeric Aβ NMR	monomeric Aβ FTIR	fibrillar Aβ NMR	fibrillar Aβ FTIR	Aβ in culture medium, FTIR
α-helix	46	44	0	5	44
β-strand	0	4	72	72	8
β-turn	45	42	13	16	36
rnd. coil	9	10	15	7	12

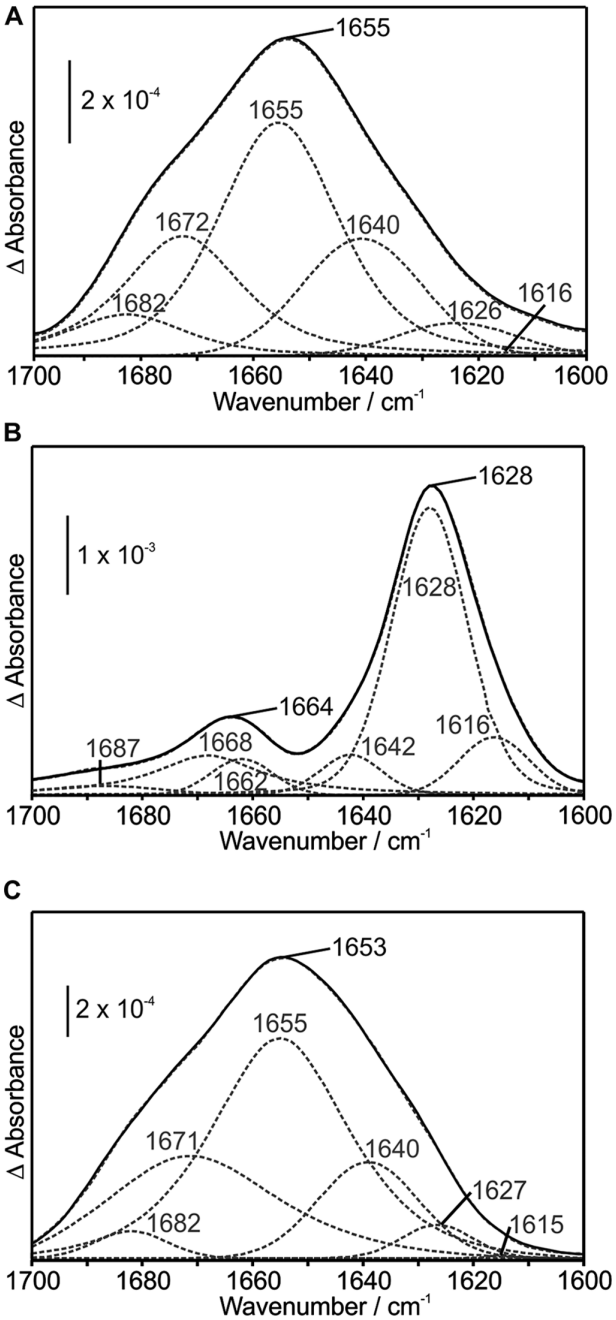

Figure 4 (**A**–**C**) The secondary structure analysis of Abeta-peptides; monomeric (**A**) and beta-sheet fibrillized synthetic Abeta (**B**). The amide I band was deconvoluted into its respective secondary structure elements, with a dominating alpha-helical component at 1655 cm^{-1} (**A**) and the dominating beta-sheet component at 1628 cm^{-1} (**B**). The amide I clearly distinguishes between alpha-helix and beta-sheet by a large downshift from 1655 to 1628 cm^{-1}. The amide I band of Abeta extracted out of chicken neuronal cell-culture medium resembled mostly monomeric Abeta peptide (**C**, also compare Table 1).

superimposed by the water band at 1640 cm^{-1} and has to be subtracted. This subtraction is less accurate at very low analyte concentrations. However, the absorbance of both bands linearly correlates with the sample concentration (Figure 5B).

The respective signal-to-noise (S/N) ratios observed in both amide I and amide II bands depict a sufficient signal with Abeta42 concentrations of 1 ng/ml with minimum values of 41 and 54 (Figure 5C).

Notably, the new sensor system did not require deuterated buffer or a deuteration of the sample to monitor the amide I band. Such a procedure would be mandatory for conventional used aqueous solution in FTIR analysis at physiological concentrations of low abundant proteins, because of the overlap of the amide I band with the O–H-bending vibration of water. The latter can be downshifted by H–D-exchange to 1210 cm^{-1} to reveal the amide I band of the desired protein. However, an H–D-exchange of a body fluid might induce unpredictable isotope effects on the contained proteins, which may also alter the secondary structure. Therefore, a reported alternative surface modification of an IRE with different geometry [67] is not applicable to body fluids.

It is important to point out, that the analyte structure in our sensor is preserved in a most native state in presence of the complex fluid in the sensor set-up. In particular, the sensor sensitivity to Abeta concentrations is well below the physiological concentration of approximately 15 ng/ml of total Abeta in human CSF. The sensor sensitivity is therefore sufficient for CSF analysis. However, for the analysis of Abeta in blood, the sensor has to be optimized with a highly-specific Abeta-antibody and the reduction of the system volume. Blood analysis would allow a routine-screening of an earlier state before clinical symptoms become evident. This is urgently desired in potential therapy.

4. Conclusion

The performance of a fast and marker-free ATR-FTIR set-up for the secondary structure analysis of Abeta peptides in the presence of a biological fluid with Abeta concentrations close to those found in CSF was presented. The successful capture of Abeta peptides was verified by simultaneous fluorescence measurements. 1 ng/ml Abeta, which is clearly below the physiological concentration of 15 ng/ml in CSF, was detected with an excellent signal-to-noise ratio.

The secondary structure analysis of Abeta selected from neuronal cell-culture medium provided a similar secondary structure as the monomeric synthetic Abeta peptide under the given measurement conditions.

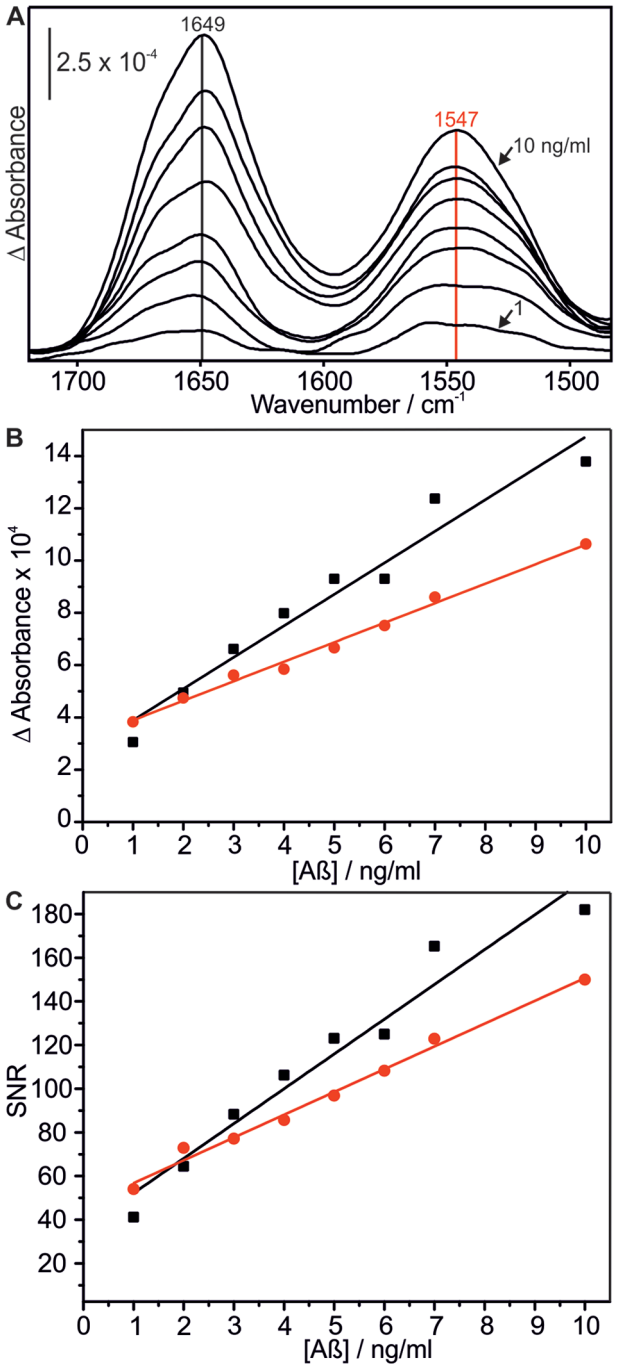

Figure 5 (**A**–**C**) The sensitivity of the immunological ATR sensor for synthetic Abeta. The amide I and amide II band intensities of synthetic Abeta monomers are shown at different concentrations from 10 ng/ml down to 1 ng/ml (**A**). The corresponding absorbance in dependence of concentration is shown in B. 1 ng/ml in the amide I (black) and II band (red) can be reliably detected (**B**). Corresponding S/N ratios of above 41 (amide I) were achieved with 1 ng/ml Abeta peptide concentration (**C**).

The set-up does neither require isolation, nor purification, nor concentration. In the next step, the set-up should be applied to body-fluids of Alzheimer disease patients. It would be challenging to see, if the Abeta transition to beta-sheet can be correlated to Alzheimer's disease. In this case, the FTIR-spectroscopic set-up might become a new diagnostic tool to identify Alzheimer's disease at an early state. Depending on the applied antibodies, e.g. against alpha-synuclein for Parkinson's disease, the set-up might be even used in other neurodegenerative diseases which are also correlated with misfolded proteins [2].

Supporting Information

Additional supporting information may be found in the online version of this article at the publisher's website.

Acknowledgements This research was supported by the Protein Research Unit Ruhr within Europe (PURE), Ministry of Innovation, Science and Research of North-Rhine Westphalia, Germany. We already filed the presented sensor for patent application (PCT/EP2015/052945).

Author biographies Please see Supporting Information online.

References

[1] T. A. Bayer, Eur. Neuropsychopharmacol. (2013).
[2] L. C. Walker and H. LeVine, Mol. Neurobiol. **21**, 83 (2000).
[3] World Health Organisation, Alzheimer's Disease International, Dementia: A Public Health Priority (World Health Organization, Geneva, 2012), pp. 1–103.
[4] R. L. Nussbaum and C. E. Ellis, N. Engl. J. Med. **348**, 1356 (2003).
[5] D. J. Selkoe, Science (New York, N.Y.) **298**, 789 (2002).
[6] J. A. Hardy and G. A. Higgins, Science **256**, 184 (1992).
[7] J. Hardy and D. J. Selkoe, Science **297**, 353 (2002).
[8] C. Reitz, International Journal of Alzheimer's Disease **2012**, 1 (2012).
[9] R. J. O'Brien and P. C. Wong, Annu. Rev. Neurosci. **34**, 185 (2011).
[10] J. Wiltfang, H. Esselmann, M. Bibl, A. Smirnov, M. Otto, S. Paul, B. Schmidt, H.-W. Klafki, M. Maler, T. Dyrks, M. Bienert, M. Beyermann, E. Rüther, and J. Kornhuber, J. Neurochem. **81**, 481 (2002).
[11] P. Lewczuk, J. Kornhuber, H. Vanderstichele, E. Vanmechelen, H. Esselmann, M. Bibl, S. Wolf, M. Otto, U. Reulbach, H. Kölsch, F. Jessen, J. Schröder, P. Schönknecht, H. Hampel, O. Peters, E. Weimer, R. Perneczky, H. Jahn, C. Luckhaus, U. Lamla, T. Supprian, J. M. Maler, and J. Wiltfang, Neurobiol. Aging **29**, 812 (2008).

[12] M. Bibl, V. Welge, H. Esselmann, and J. Wiltfang, Electrophoresis **33**, 445 (2012).
[13] M. I. Rosa, J. Perucchi, L. R. Medeiros, B. Fernandes, M. E. Fernandes Dos Reis, and B. R. Silva, J. Alzheimers Dis. **40**, 443 (2014).
[14] A. M. Fagan, M. A. Mintun, R. H. Mach, S.-Y. Lee, C. S. Dence, A. R. Shah, G. N. LaRossa, M. L. Spinner, W. E. Klunk, C. A. Mathis, S. T. DeKosky, J. C. Morris, and D. M. Holtzman, Ann. Neurol. **59**, 512 (2006).
[15] N. Tolboom, W. M. van der Flier, M. Yaqub, R. Boellaard, N. A. Verwey, M. A. Blankenstein, A. D. Windhorst, P. Scheltens, A. A. Lammertsma, and B. N. M. van Berckel, J. Nucl. Med. **50**, 1464 (2009).
[16] J. T. Jarrett and P. T. Lansbury, Cell **73**, 1055 (1993).
[17] I. Benilova, E. Karran, and B. De Strooper, Nat. Neurosci. **15**, 349 (2012).
[18] L. Milanesi, T. Sheynis, W.-F. Xue, E. V. Orlova, A. L. Hellewell, R. Jelinek, E. W. Hewitt, S. E. Radford, and H. R. Saibil, Proc. Natl. Acad. Sci. U.S.A. **109**, 20455 (2012).
[19] I. Zawisza, M. Rózga, and W. Bal, Coord. Chem. Rev. **256**, 2297 (2012).
[20] M. Fändrich, J. Meinhardt, and N. Grigorieff, Prion **3**, 89 (2009).
[21] C. Sachse, M. Fändrich, and N. Grigorieff, Proc. Natl. Acad. Sci. U.S.A. **105**, 7462 (2008).
[22] C. G. Glabe, J. Biol. Chem. **283**, 29639 (2008).
[23] C. Kötting and K. Gerwert, Chemphyschem **6**, 881–888 (2005).
[24] F. Garczarek and K. Gerwert, Nature **439**, 109–112 (2006).
[25] S. Krimm, Biopolymers **22**, 217 (1983).
[26] S. Krimm and J. Bandekar, Adv. Protein Chem. **38**, 181 (1986).
[27] H. Susi and D. M. Byler, Biochem. Biophys. Res. Commun. **115**, 391–397 (1983).
[28] H. Susi, D. M. Byler, and J. M. Purcell, J. Biochem. Biophys. Methods **11**, 235–240 (1985).
[29] D. M. Byler and H. Susi, Biopolymers **25**, 469–487 (1986).
[30] E. Goormaghtigh, V. Cabiaux, and J. M. Ruysschaert, Eur. J. Biochem. **193**, 409–420 (1990).
[31] J. Ollesch, E. Künnemann, R. Glockshuber, and K. Gerwert, Appl. Spectrosc. **61**, 1025–1031 (2007).
[32] H. Fabian, K. Gast, M. Laue, K. J. Jetzschmann, D. Naumann, A. Ziegler, and B. Uchanska-Ziegler, Biophys. Chem. **179**, 35 (2013).
[33] K. Elfrink, J. Ollesch, J. Stöhr, D. Willbold, D. Riesner, and K. Gerwert, Proc. Natl. Acad. Sci. U.S.A. **105**, 10815–10819 (2008).
[34] J. Kneipp, M. Beekes, P. Lasch, and D. Naumann, J. Neurosci. **22**, 2989 (2002).
[35] A. Kretlow, Q. Wang, J. Kneipp, P. Lasch, M. Beekes, L. Miller, and D. Naumann, Biochim. Biophys. Acta **1758**, 948–959 (2006).
[36] A. Kretlow, Q. Wang, M. Beekes, D. Naumann, and L. M. Miller, Biochim. Biophys. Acta **1782**, 559 (2008).
[37] Robert Koch Institut, 13353 Berlin, DE, [An Apparatus for Diagnosing TSE-Induced Changes in Tissues by Means of Infrared Spectroscopy] (DE20023042U1, 2002).
[38] E. Baldauf, M. Beekes, J. Kneipp, P. Lasch, and D. Naumann, Method for Diagnosing Tse-Induced Changes in Tissues Using Infrared Spectroscopy (EP1181552 (A2), 2003).
[39] D. Naumann, J. Kneipp, E. Baldauf, P. Lasch, and M. Beekes, Fast Detection of Pathologic Changes Induced by Transmissible Spongiform Encephalopathies (tse) in Animal or Human Tissue Using Infrared Spectroscopy (ir Spectroscopy) (US6777241 B1, 2004).
[40] H. U. Gremlich, U. P. Fringeli, and R. Schwyzer, Biochemistry **22**, 4257 (1983).
[41] P. Wenzl, M. Fringeli, J. Goette, and U. P. Fringeli, Langmuir **10**, 4253 (1994).
[42] L. K. Tamm and S. A. Tatulian, Q. Rev. Biophys. **30**, 365–429 (1997).
[43] E. Goormaghtigh, V. Raussens, and J.-M. Ruyschaert, Biochim. Biophys. Acta **1422**, 105 (1998).
[44] S. A. Tatulian, Biochemistry **42**, 11898 (2003).
[45] J. Ollesch, B. C. Poschner, J. Nikolaus, M. W. Hofmann, A. Herrmann, K. Gerwert, and D. Langosch, Eur. Biophys. J. **37**, 435–445 (2008).
[46] L. K. Tamm and J. T. Groves, J. Struct. Biol. **168**, 1 (2009).
[47] P. Pinkerneil, J. Güldenhaupt, K. Gerwert, and C. Kötting, Chemphyschem **13**, 2649 (2012).
[48] R. Adato and H. Altug, Nat. Commun. **4**, 2154 (2013).
[49] A. De Ninno, G. Ciasca, A. Gerardino, E. Calandrini, M. Papi, M. De Spirito, A. Nucara, M. Ortolani, L. Businaro, and L. Baldassarre, Phys. Chem. Chem. Phys., DOI: 10.1039/c4cp05023a (2015).
[50] M. Voue, E. Goormaghtigh, F. Homble, J. Marchand-Brynaert, J. Conti, S. Devouge, and J. De Coninck, Langmuir **23**, 949 (2007).
[51] J. Schartner, K. Gavriljuk, A. Nabers, P. Weide, M. Muhler, K. Gerwert, and C. Kötting, Chembiochem **15**, 2529 (2014).
[52] J. Schartner, J. Güldenhaupt, B. Mei, M. Rögner, M. Muhler, K. Gerwert, and C. Kötting, J. Am. Chem. Soc. **135**, 4079 (2013).
[53] E. Goormaghtigh, J.-M. Ruysschaert, and V. Raussens, Biophys. J. **90**, 2946 (2006).
[54] S. C. Gill and P. H. von Hippel, Anal. Biochem. **182**, 319 (1989).
[55] H. Schieb, S. Weidlich, G. Schlechtingen, P. Linning, G. Jennings, M. Gruner, J. Wiltfang, H.-W. Klafki, and H.-J. Knölker, Chemistry **16**, 14412 (2010).
[56] J. Wiltfang, H. Esselmann, P. Cupers, M. Neumann, H. Kretzschmar, M. Beyermann, D. Schleuder, H. Jahn, E. Rüther, J. Kornhuber, W. Annaert, B. De Strooper, and P. Saftig, J. Biol. Chem. **276**, 42645 (2001).
[57] T. S. A. Dyrks, U. D. S. A. Mönning, and J. D. Wiltfang, EP1270592 B1 (September 2004).
[58] M. Schmidt, C. Sachse, W. Richter, C. Xu, M. Fändrich, and N. Grigorieff, Proc. Natl. Acad. Sci. U.S.A. **106**, 19813 (2009).
[59] G. Zandomeneghi, M. R. H. Krebs, M. G. McCammon, and M. Fändrich, Protein Sci. **13**, 3314 (2004).
[60] I. Morgado, K. Wieligmann, M. Bereza, R. Ronicke, K. Meinhardt, K. Annamalai, M. Baumann, J. Wacker, P. Hortschansky, M. Malesevic, C. Parthier, C. Ma-

wrin, C. Schiene-Fischer, K. G. Reymann, M. T. Stubbs, J. Balbach, M. Gorlach, U. Horn, and M. Fandrich, Proc. Natl. Acad. Sci. U.S.A. **109**, 12503 (2012).

[61] B. Strodel, J. W. L. Lee, C. S. Whittleston, and D. J. Wales, J. Am. Chem. Soc. **132**, 13300 (2010).

[62] L. Yu, R. Edalji, J. E. Harlan, T. F. Holzman, A. P. Lopez, B. Labkovsky, H. Hillen, S. Barghorn, U. Ebert, P. L. Richardson, L. Miesbauer, L. Solomon, D. Bartley, K. Walter, R. W. Johnson, P. J. Hajduk, and E. T. Olejniczak, Biochemistry **48**, 1870 (2009).

[63] S. Vivekanandan, J. R. Brender, S. Y. Lee, and A. Ramamoorthy, Biochem. Biophys. Res. Commun. **411**, 312 (2011).

[64] S. Zhang, K. Iwata, M. J. Lachenmann, J. W. Peng, S. Li, E. R. Stimson, Y. Lu, A. M. Felix, J. E. Maggio, and J. P. Lee, J. Struct. Biol. **130**, 130 (2000).

[65] N. Rezaei-Ghaleh, M. Amininasab, K. Giller, S. Kumar, A. Stündl, A. Schneider, S. Becker, J. Walter, and M. Zweckstetter, J. Am. Chem. Soc. **136**, 4913 (2014).

[66] H. Esselmann, J. M. Maler, N. Kunz, M. Otto, S. Paul, P. Lewczuk, E. Rüther, J. Kornhuber, and J. Wiltfang, Neurodegener Dis **1**, 236 (2004).

[67] E. Kleiren, J.-M. Ruysschaert, E. Goormaghtigh, and V. Raussens, Spectrosc.-Int. J. **24**, 61 (2010).

Supplement:

An infrared sensor analysing label-free the secondary structure of the Abeta peptide in presence of complex fluids

Andreas Nabers[1,3], Julian Ollesch[1,3], Jonas Schartner[1], Just Genius[2], Ute Haußmann[2], Hans Klafki[2], Carsten Kötting[1], Jens Wiltfang[2], Klaus Gerwert[1]

Schematics of the sensor

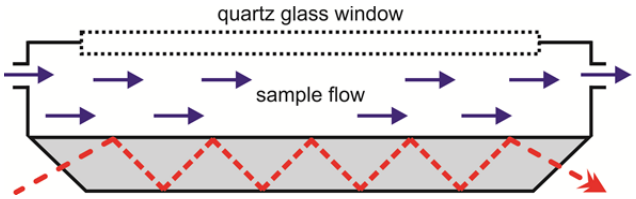

Supplementary Figure 1 Schematics of the sensor element. The germanium IRE (grey) is mounted in a flow-through cuvette. The casing features a quartz glass window for optional fluorescence analysis. The sample flow (blue arrows) through the cuvette is controlled with a peristaltic pump.

The signal to noise ratio (S/N) was calculated with a spectroscopic standard procedure: two single channel spectra I_0 and I were subsequently recorded of the receptive and blocked sensor element. The transmission spectrum $T=I/I_0$ was calculated. The root mean squared noise value (N_{RMS}) was calculated for the wavenumber range $\nu \in \{1700cm^{-1}..1600cm^{-1}\}$ with

$$N_{RMS} = \sqrt{1/n \sum_{i=1}^{n} (1 - T(\nu_i))^2}$$

using the spectrometer software (Bruker OPUS) internal function. Then, S/N was calculated as maximum signal intensity of the absorbance spectrum divided by the noise level.

Long-term-stability

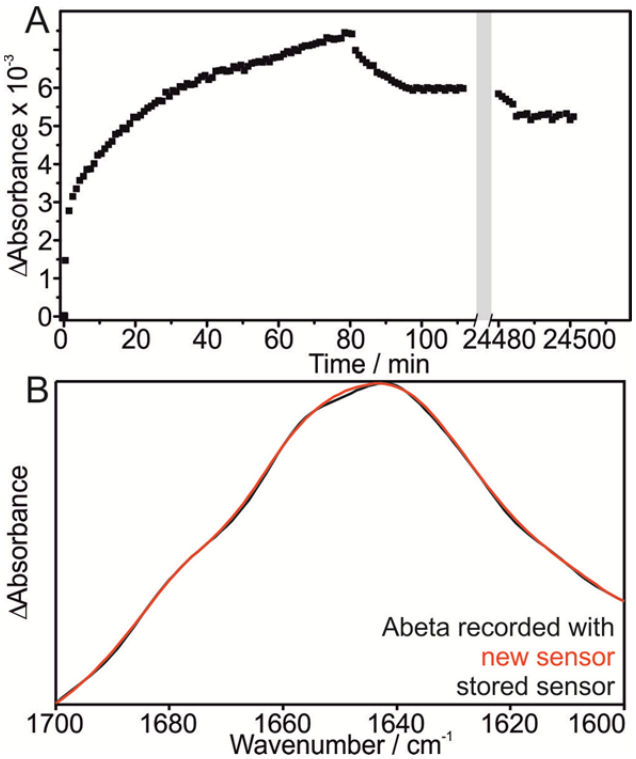

Supplementary Figure 2 Long term stability of the prepared sensor element was evaluated with one antibody coated sensor stored outside the spectrometer at 4°C for 17 days. The amide II band at 1550 cm^{-1} was followed over time (A). After storage, the spectrum recording was resumed at room temperature. Only minimal dissociation from the surface was observed with prolonged rinsing. The scaled Abeta peptide absorbance spectra recorded with the stored and a freshly prepared sensor demonstrate extreme reproducibility (B).

Cross-reactivity

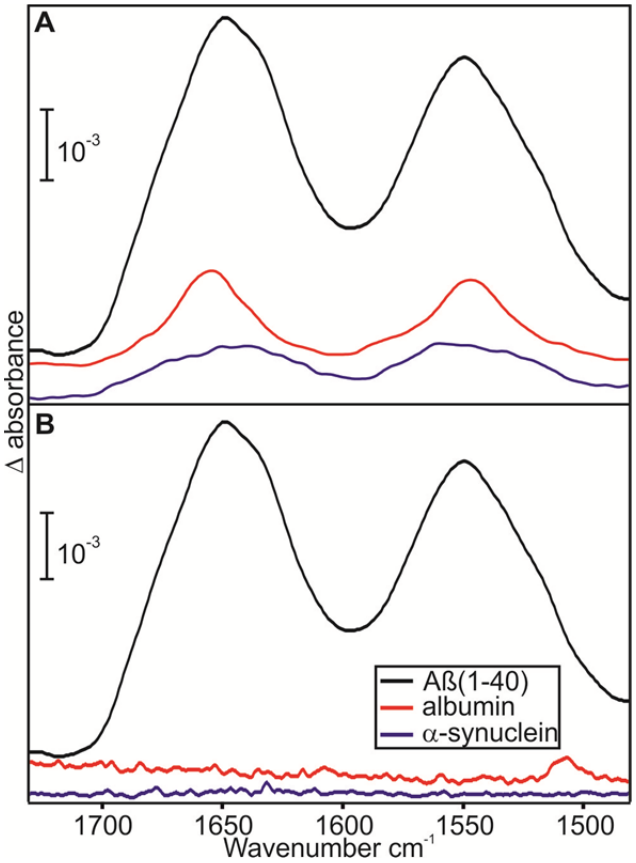

Supplementary Figure 3 Cross-reactivity of the sensor surface with albumin and α-synuclein as two selected blood components. Albumin is the most abundant blood protein, whereas α-synuclein represents another amyloidogenic protein. An unblocked sensor surface is receptive for α-synuclein incubated at 20 ng/ml (blue), albumin incubated at 25 µg/ml concentration (red), and Abeta1-40 peptide incubated at 15 ng/ml concentration (A). The blocked sensor was not receptive except for Abeta1-40 peptide (B, black). Spectra have been offset for comparability.

Reproducibility

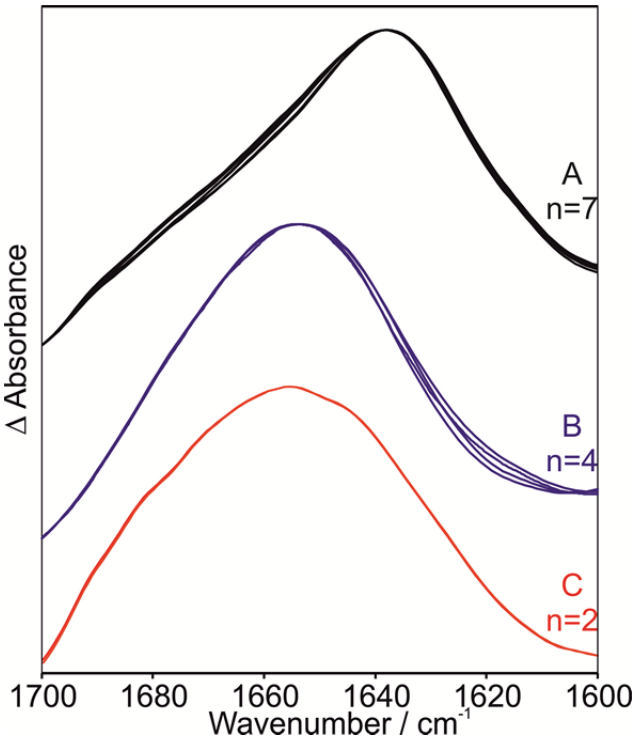

Supplementary Figure 4 The amide I bands recorded from n separately prepared sensors binding antibody 1E8 onto silane (A), casein binding onto antibody loaded sensors (B), and Abeta peptide captured from chicken neuroblast cell culture medium (C, sample taken from another cell culture as analysed in the manuscript and suppl. Fig. 5) indicate an excellent spectral reproducibility. Spectra were obtained as differences from a buffer rinsed reference state before and a buffer rinsed sample state after substance application into the flow system. The antibody secondary structure is preserved, although the covalent antibody binding is not limited to a particular epitope besides accessible primary amines. The Abeta peptide absorbance spectra reproducibility is excellent.

Determination of the dominating Abeta conformation as excreted out of neuronal cells

The amide I band of Abeta extracted out of neuronal cell culture media, Fig. 4 C, was decomposed as a linear combination of monomeric (Fig. 4 A) and fibrillar Abeta proteins (Fig. 4 B). There is no oligomeric Abeta spectrum available as reference. The secondary structure analysis of these two Abeta conformations by IR was compared to NMR analysis- of Abeta monomers (PDB 1Z0Q) and fibrils (PDB 2BEG) and showed good agreement. 96 % of the cell culture amide I band agrees with synthetic Abeta proteins, with 92 % monomeric and 4 % fibrillar fold, respectively. The remaining fraction of 4 % covered by the residual spectrum indicated the possible presence of other, maybe oligomeric conformations or Abeta related proteins that also can crossreact with the 1E8 antibody.

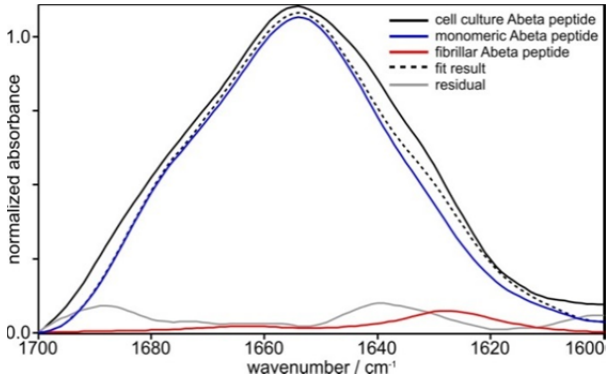

Supplementary Figure 5 The absorbance spectrum obtained from chicken neuronal cell culture (Fig. 4 C) as a linear combination of monomeric and fibrillar synthetic Abeta protein (Fig. 4 A, B) results in a distribution of 92 % monomeric, and 4 % fibrillar protein. A residual of 4% indicates at least a third conformation present in the spectrum.